Progress in Nuclear Energy 89 (2016) 120–131

Contents lists available at ScienceDirect

Progress in Nuclear Energy

journal homepage: www.elsevier.com/locate/pnucene

Numerical simulation of bubble condensation using CF-VOF

N. Samkhaniani, M.R. Ansari*

Faculty of Mechanical Engineering, Tarbiat Modares University, P.O. Box 14117 13116, Tehran, Islamic Republic of Iran

ARTICLE INFO

Article history:
Received 3 November 2015
Received in revised form
27 January 2016
Accepted 3 February 2016
Available online 23 February 2016

Keyword:
Condensation
Subcooled boiling
VOF
OpenFOAM
Bubble

ABSTRACT

In present study, subcooled boiling is simulated using color function volume of fluid (CF-VOF) method. To this purpose, energy equation and Tanasawa mass transfer model accompanied with some suitable source terms are implemented in OpenFOAM solver (interFoam). The surface tension between vapor and liquid phases is considered using continuous surface force (CSF) method. In order to reduce spurious current near interface, a smoothing filter is applied to improve curvature calculation. The variation of saturation temperature in vapor bubble with local pressure is considered with Clausius–Clapeyron relation. The numerical model is validated with one-dimensional Stefan problem.

The bubble shape and life time history of single vapor bubble condensation are verified with existing experimental data. Computational study shows bubble life time is nearly proportional with bubble size and it is prolonged at bubble swarm motion. The present study reveals some fundamental characteristics of single and multiple vapor bubble condensation and is expected to be instructive for further applications.

1. Introduction

The bubble condensation is one of the fundamental issues in the subcooled flow boiling to describe the heat and mass transfer. It is encountered in many industrial applications such as nuclear reactors. For nuclear reactors, the bubble dynamics can greatly influence the reactivity feedback characteristics of coolant which brings more challenges for reactor safety analysis. The bubble size, bubble shape and void fraction change continuously in bubble condensing process, and it affects flow structure around bubble. In order to understand the subcooled flow boiling, it is a challenge to obtain an extensive knowledge on the condensing bubbles behavior.

There have been many experimental analyses on the condensing bubble behavior (Kamei and Hirata, 1990a,b; Sideman and Hirsch, 1965; Sudhoff et al., 1982). In experimental investigations, visualization is a common method to analyze the bubble condensing process. The surface area, volume and vapor content of a rising bubble are determined through visualization. Sideman and Hirasch (Sideman and Hirsch, 1965) studied free rising of the isopentane condensing bubbles at subcooled water. Kamei and Hitara have analyzed the bubble deformation and life time (Kamei and Hirata, 1990a,b). Chen and Mayinger (Chen and Mayinger, 1992) studied the heat transfer at the interface of condensing vapor bubble in a subcooled liquid of the same substances with ethanol, propane, R113 and water. Harada (Harada et al., 2010) carried out the visualization experiments to investigate the dynamics of vapor bubbles generated in water pool boiling. In the experimental studies, bubble behavior with bubble size history, shape, velocity, collapse time and interfacial heat transfer coefficient was investigated in quiescent (Brucker and Sparrow, 1977) and upward flow (Lucas and Prasser, 2007). It was found that the collapsing points of time and height are proportional with the variation of pressure and temperature difference in quiescent liquid (Brucker and Sparrow, 1977). Bubble collapse during condensation in immiscible liquids can be controlled either by inertia or by heat transfer mechanisms. At a high subcooled temperature, bubble rapidly collapses. This process controlled by inertial. On the other hand, if subcooled temperature is relatively low, the bubble life time is longer and the process will be controlled by the heat transfer at the interface. The bubble collapse rate is generally assumed to be controlled by the internal, external thermal resistances and the temperature driving force. However, it can be affected by many parameters such as: working fluid, miscibility, bubble shape, bubble size, fraction of non-condensable gases, surface mobility and etc. For short duration of experiment and complexity of phenomenon, it is impossible to obtain detailed information about condensing process through

* Corresponding author.
E-mail addresses: nima.samkhaniani@gmail.com (N. Samkhaniani), mra_1330@modares.ac.ir (M.R. Ansari).

http://dx.doi.org/10.1016/j.pnucene.2016.02.004
0149-1970/

Nomenclature

C_α	Compression factor, –
C_p	Specific heat, J/kgK
d_L	Liquid thermal diffusivity: $k/\rho C_p$, m^2/s
D	Equivalent diameter, m
D_0	Bubble Initial diameter, m
$\vec{g}$	gravity acceleration, m/s^2
H_{LG}	Latent heat, J/kg
k	Thermal conductivity, W/mK
M	Molar mass, Kg/Kmol
$\dot{m}'''$	Condensate mass flow rate per unit volume, Kg/m^3s
P	Pressure, Pa
P_{rgh}	Dynamic Pressure, Pa
R	Universal gas constant, J/mol K
T	Temperature, K
$\vec{U}$	velocity, m/s
$\vec{U_b}$	Bubble velocity, m/s
$\vec{U_c}$	Compressive velocity, m/s
$\vec{U_r}$	Relative velocity, m/s

Greek symbols

α	Volume fraction factor
κ	Interface curvature, m^{-1}
μ	Dynamic viscosity, Pa s
ρ	Density, Kg/m^3

Subscripts

G	Gas (vapor) phase
L	Liquid phase
sat	Saturation condition
sub	Subcooled condition

09 Longkai GUO

experimental because the shape and the area of bubble interface are exposure of rapid changes. Therefore, numerical simulation of condensing bubble is vital as complement to experiments. Tian et al. (Tian et al., 2010) simulated single steam bubble condensation behaviors in subcooled water using the Moving Particle Semi-implicit (MPS) method in axisymmetric domain. Chen et al. (2010); Chen et al. (2011) applied MPS method in 2-dimensional domain for simulation of pair bubble rising in stagnant liquid and simulation of nucleating boiling in subcooled liquid. Pan et al. (Pan et al., 2012) numerically investigated the behavior of condensing single vapor bubble in subcooled boiling flow within two different vertical rectangular channels using the Volume of Fluid (VOF) multiphase flow model. Zeng et al. (2015) investigated the bubble condensation process for different initial bubble sizes and subcooled temperatures using the couple of level set method (LS) and volume of fluid (VOF) in 3D domain.

10-11 2 notes:

present study, the vapor bubble condensing process in quiescent water is simulated using volume of fluid method in OpenFOAM CFD package (H. G. Weller et al., 1998). The OpenFOAM library allows implementations of fields, equations and operator discretization using high level C++(Weller et al., 1998). In the previous study VOF method in interFoam solver has been used to simulate single bubble rising (Samkhaniani et al., 2012). Deshpande et al. (Deshpande et al., 2012) evaluate the performance of this solver using a variety of verification and validation test cases and found out interFoam is generally comparable with the recent algebraic VOF algorithms. In order to simulate phase change process in bubble condensation phenomena, interFoam solver in OpenFOAM220 is extended to solve energy equation and calculate mass flux.

12 Longkai GUO

2. Mathematical model

2.1. Governing equation

In present study, the two phase flow is treated as incompressible and immiscible Newtonian fluid. Interface between two phases are resolved using color function volume of fluid method (CF-VOF). Following discontinuous scalar function is applied for interface tracking in fixed Eulerian grids. This scalar function is the ratio of one fluid volume to the volume of cell and defined as:

$$\alpha_L(\vec{x},t)=\frac{V_{Liquid}}{V}=\begin{cases}1 & \vec{x}\in\text{Liquid}\\ 0<\alpha_L<1 & \vec{x}\in\text{interface}\\ 0 & \vec{x}\in\text{gas}\end{cases} \tag{1}$$

The thermo physical properties of two immiscible fluids such as viscosity (μ), density (ρ) and thermal conductivity (k) are calculated using a weighted average:

$$y=\alpha_L y_L+(1.0-\alpha_L)y_G,\qquad y\in[\rho,\mu,k] \tag{2}$$

The global continuity equation of two phase flow is given by:

$$\frac{\partial}{\partial t}(\rho)+\nabla\cdot(\rho\vec{U})=0 \tag{3}$$

In two phase flow, the interface moves with flow. Thus, the transport equation should be solved for VOF function to keep interface. This transport equation is derived from global continuity equation by substitution of density from equation (2) and defined as:

$$\frac{\partial\alpha_L}{\partial t}+\vec{U}\cdot\nabla\alpha_L+\alpha_L\nabla\cdot\vec{U}=-\frac{\rho_G\nabla\cdot\vec{U}}{(\rho_L-\rho_G)} \tag{4}$$

where $\nabla\cdot\vec{U}$ is calculated from local continuity equations for each phase:

$$\nabla\cdot\vec{U}=\dot{m}'''\left(\frac{1}{\rho_G}-\frac{1}{\rho_L}\right) \tag{5}$$

where $\dot{m}'''$ (kg/m^3s) is volumetric transferred mass rate. Momentum equations are given by:

$$\frac{\partial(\rho\vec{U})}{\partial t}+\nabla\cdot(\rho\vec{U}\vec{U})-\nabla\cdot\left(\mu\left(\nabla\vec{U}^T+\nabla\vec{U}\right)\right)=-\nabla P+\rho\vec{g}+\sigma\kappa\nabla\alpha_L \tag{6}$$

Last term in right hand of equation (6) indicates surface tension force between two phases. σ is surface tension and κ is interface curvature. The surface tension is accounted by Continuum Surface Force model (CSF) without the density averaging proposed by (Brackbill et al., 1992). Curvature is defined as:

$$\kappa = -\nabla\cdot\left(\frac{\nabla\widetilde{\alpha_L}}{|\nabla\widetilde{\alpha_L}|}\right) \tag{7}$$

where $\widetilde{\alpha_L}$ is calculated from the VOF fu[illegible]n α by smoothing it over a finite region around the interface. In the VOF method, the fluid interface sharply changes over a thin region. This abrupt change of the VOF function creates errors in calculating the normal vectors and the curvature of the interface, which are used to evaluate the interfacial forces. These errors induce non-physical spurious currents in the interfacial region (Klostermann et al., 2013; Scardovelli and Zaleski, 1999). The spurious currents create extra heat convection around interface which increases local mass transfer. An easy way to suppress these artifacts is to compute the interface curvature from a smoothed VOF function. In this study the smoother proposed by Lafaurie et al.(Lafaurie et al., 1994) is applied:

$$\widetilde{\alpha_p} = \frac{\sum_{f=1}^{n}\alpha_{Lf}S_f}{\sum_{f=1}^{n}S_f} \tag{8}$$

where S_f is the magnitude of face area, the subscript P denotes the cell index and f denotes the face index. The interpolated value (α_{Lf}) at the face centre is calculated using linear interpolation. The application of this filter can be repeated m times to get a smoothed field. It should be stressed that smoothing tends to level out high curvature regions and should therefore be applied only up to the level that is strictly necessary to sufficiently suppress parasitic currents. Hoang et al. (Hoang et al., 2013) found that the magnitude of parasitic current decreases up to one order from $m = 0$ to $m = 2$ and only a slight further decrease was observed for $m > 2$. Therefore, in present study $m = 2$ is employed in all simulations.

Energy equation is given by:

$$\frac{\partial}{\partial t}(\rho C_p T) + \nabla\cdot(\rho C_p U T) - \nabla\cdot(k\nabla T) = -\dot{m}'''(H_{LG} + (C_{pL} - C_{pG})T_{Sat}) \tag{9}$$

The term in the right hand of equation is due to phase change. H_{LG} is the latent heat coefficient. The transferred mass flux should be computed using an appropriate mass transfer model. In this study phase change model proposed by Tanasawa (Tanasawa, 1991) is employed. Mass flux (kg/m^{2}s) at the liquid vapor interface is calculated as:

$$\dot{m}'' = \frac{2\gamma}{\gamma - 1}\sqrt{\frac{M}{2\pi R}}\frac{\rho_G H_{LG}(T - T_{sat})}{T_{sat}^{3/2}} \tag{10}$$

where M is molar mass of fluid, $R = 8.314$ J/mol K is the universal gas constant, $T_{Sat}(P)$ is local saturation temperature, and γ is the fraction of molecules transferred from one phase to the other during phase change. Marek and Straub (Marek and Straub, 2001) determined γ based on published data. They recommended $\gamma = 0.1 - 1$ for dynamically renewing water surfaces such as jets or moving films, and $\gamma < 0.1$ for stagnant surfaces. More details on the different phase change model can be found in (H. Lee et al., 2015). For equations (5) and (9), the volumetric mass source term in kg/m^{3}s is needed which is determined from:

$$\dot{m}''' = \dot{m}''\nabla\alpha_L \tag{11}$$

The variation of saturation temperature based on local pressure P is calculated using a simplified version of Clausius–Clapeyron equation. It is assumed that the vapor phase in saturation temperature has an ideal gas behavior.

$$\ln\frac{P_{sat,1}}{P_{sat,0}} = -\frac{MH_{LG}}{R}\left(\frac{1}{T_{sat,1}} - \frac{1}{T_{sat,0}}\right) \tag{12}$$

2.2. Numerical details

The present solver is implemented using OpenFOAM finite volume library (H. G. Weller et al., 1998). It is based on interFoam solver. This solver supports simulation of incompressible two phase adiabatic flows without phase change using algebraic VOF. In order to simulate the subcooled flow boiling, the base solver is extended by adding a thermal energy transport equation and modifying the [illegible] solver (the volume fraction transport equation and momentum equations) with phase-change source terms. The overall solver algorithm can be described in following steps:

1. Define vector and scalar fields for the multiphase flow problem including: $\vec{U}$, P, T and α_L.Note that pressure used in the VOF solver is the dynamic pressure P_{rgh} where $P_{rgh} = P - \rho gh$, where h is the liquid height.P_{rgh} is used to avoid any sudden changes in the pressure at the boundaries for hydrostatic problems (Rusche, 2003)
2. Start the time loop and solve the volume fraction advection.

The base solver uses algebraic VOF which means no interface reconstruction method is employed to locate the exact position of interface in each cell. Therefore, the interface is diffuse among two or three cells. In order to limits the smearing of the interface because of the compensation of the diffusive fluxes. The extra divergence term $\nabla\cdot(\alpha_L(1-\alpha_L)\overrightarrow{U_c})$ is added to equation (4), which contributes only in the region of the interface ($0 < \alpha_L < 1.0$) and diminishes in liquid or vapor phases.

$$\frac{\partial\alpha_L}{\partial t} + \vec{U}\cdot\nabla\alpha_L + \nabla\cdot\left(\alpha_L(1-\alpha_L)\overrightarrow{U_c}\right) = -\dot{m}'''\left[\frac{1}{\rho_L} - \alpha_L\left(\frac{1}{\rho_L} - \frac{1}{\rho_G}\right)\right] \tag{13}$$

$\overrightarrow{U_c}$ is compressive velocity. It is calculated in the normal direction of the interface to avoid any dispersion. Moreover, a compressive factor (C_α) is used to increase compression:

$$\overrightarrow{U_c} = \min\{C_\alpha|U|, \max(|U|)\}\frac{\nabla\alpha_L}{|\nabla\alpha_L|} \tag{14}$$

In present study the compression factor $C_\alpha = 1.0$ is considered. The coefficient C_α controls the weight of the compression flux and should be usually in the range of unity ($1.0 < C_\alpha < 4.0$) (Berberović et al., 2009; Samkhaniani et al., 2013).

The volume fraction advection equation is solved using the multidimensional universal limiter with explicit solution (MULES) method which is based on the method of flux corrected transport (FCT) (Zalesak, 1979) where an additional limiter is used to cutoff the face-fluxes at the critical values. This solver is included in OpenFOAM library, and performs conservative transport equation of hyperbolic transport equations with defined bounds (0 and 1 forα_L).

3. Update the fluid physical properties and the fluxes using the volume fraction function α_L using equation (2).
4. Solve the Navier Stokes system of equations for velocity and pressure using the Pressure Implicit with Splitting of Operators (PISO) (Issa et al., 1986). In the present study, three pressure

Table 1
Discretisation schemes.

Term	Discretisation scheme	Method
$\frac{\partial}{\partial t}(\rho\vec{U}), \frac{\partial}{\partial t}(\rho\vec{U}T)$	Euler	the first order bounded implicit scheme
$\nabla\cdot(\rho\vec{U}\vec{U})$	vanLeerV	Similar to VanLeer scheme (Van Leer, 1974) modified for vector field
$\nabla\cdot(\vec{U}\alpha_L)$, $\nabla\cdot(\rho\vec{U}T)$	vanLeer	See (Van Leer, 1974)
$\nabla\cdot(\vec{U_c}\alpha_L(1-\alpha_L))$	InterfaceCompression	See (H. Weller, 2008)
$\nabla\chi^*$	Linear	central difference schemes
$\nabla^{**}_{\vec{f}}\chi$	corrected	surface normal gradient with correction on non-orthogonal meshes (Jasak, 1996)
$\nabla\cdot(\chi_1\nabla\chi_2)$	Linear corrected	face values (χ_1) approximated by central difference scheme, and the resulting surface normal gradient is calculated using central difference schemes with non-orthogonal correction
Term	**Interpolation scheme**	**Method**
χ_f	Linear	Default interpolation schemes for getting face values from cell values

21-22
2 notes:

ction steps were used and ensured that the pressure re- ual remained always below 10^{-10}.

First, the matrix equation for the momentum equation is formed. Then the inner pressure–velocity correction process is initiated. In PISO, an intermediate velocity field is first obtained, and the cell-face volume fluxes (ϕ) are evaluated and corrected for gravitational forces, the continuum surface-tension force, and boundary conditions. The pressure–Poisson equation is then formed and solved. Following the approach of (Weller et al., 1998), the coefficients of the pressure equation are obtained from the nal entries of the momentum matrix equation (A_D). For pre- condensing flows, the pressure equation would be:

23

Longkai GUO

$$\nabla\cdot\left(\frac{1}{A_D}\nabla P_{rgh}\right) = \nabla\cdot\phi - \dot{m}'''\left(\frac{1}{\rho_G}-\frac{1}{\rho_L}\right) \tag{15}$$

where the last term in the right hand of equation (15) is added to consider phase change process. T essure correction equation is solved in present study using a ugate gradient iterative (PCG) solver preconditioned with a geometric algebraic multi grid method (GAMG).

24-25
2 notes:

5. Solve energy Equation for temperature

The numerical interfacial flow computations become more enging when the imbalance of material properties between phases increases (Scardovelli and Zaleski, 1999). In order to reduce material properties imbalance through interface and increase numerical robustness, equation (9) is redefined as:

26

Longkai GUO

$$\frac{\partial}{\partial t}(T) + \nabla\cdot(UT) - \nabla\cdot(D_k\nabla T) = \dot{m}'''(H_{LG} + (C_{pL} - C_{pG})T_{sat}) \tag{16}$$

where D_k and D_c are defined as:

$$D_c = \frac{1}{\rho_L C_L\alpha_L + \rho_G C_G(1-\alpha_L)} \tag{17}$$

$$D_k = \frac{k_L\alpha_L + k_G(1-\alpha_L)}{\rho_L C_L\alpha_L + \rho_G C_G(1-\alpha_L)} \tag{18}$$

6. Move to the next time step (starting from 2).

For the stability of the solution procedure, the calculations are performed using a self-adapting time step based on the user defined maximum Courant number (Co_{max}) and maximum time step (Δt_{max}) (Berberović et al., 2009). Here, $Co_{max} = 0.1$ is employed for all simulations.

The governing equations are discretized based on a finite volume method (FVM) formulation. The discretization is performed on a structu rid. All the variables are stored at the cell centers, where a cated grid arrangement is used. In order to avoid a checker boarding effect in the momentum equation, the Rhie-Chow momentum interpolation (Rhie and Chow, 1983) is employed.

The applied discretisation schemes and the parameters of the numerical model are summarized in Table 1. For convenience, the corresponding terminology of OpenFOAM is given.

2.3. Validation of phase change model

The one dimensional Stefan problem was introduced for

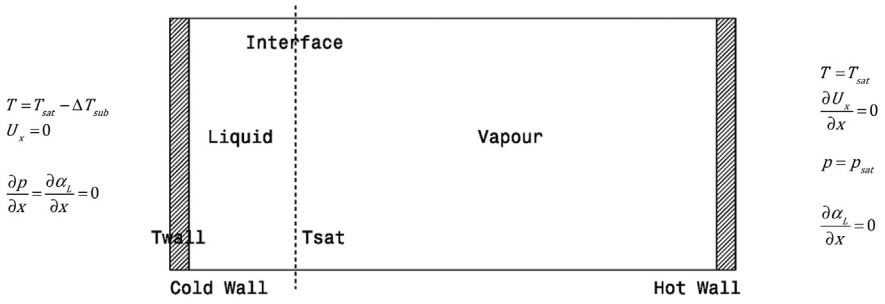

Fig. 1. Schematic of Stefan problem and boundary conditions, $T_{Sat} = 380.26$[K], $\Delta T_{sub} = 10$[K], $C_{pG} = C_{pL}(p_{sat})$.

Table 2
Water thermo physical properties at saturation temperature (P_{sat} = 0.130 MPa, T_{sat} = 380.26).

	Dimension	Liquid	Vapor
Density	Kg/m^3	953.13	0.75453
Viscosity	Pa.s	2.6E-04	1.25E-05
Thermal conductivity	W/mK	0.68106	0.025905
Specific Heat	kJ/kgK	4.224	2.110
Latent Heat	kJ/kg	2237.41	
Surface Tension	N/m	0.05753	

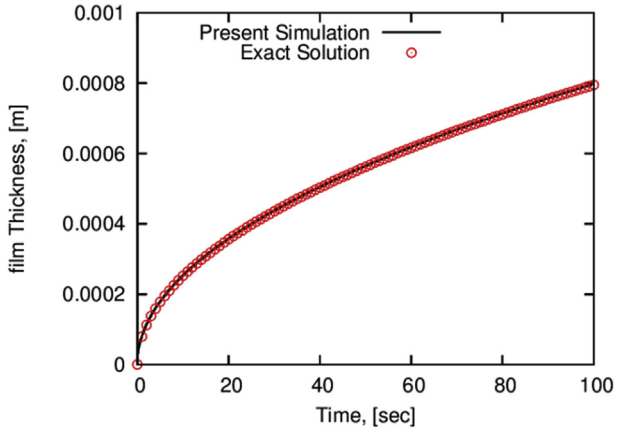

Fig. 2. Stefan problem, comparison between analytical solution and CFD model, P_{sat} = 0.130 MPa and ΔT = 10 K.

Table 3
Stefan problem convergence.

	64	128	256	512	Exact
$\delta(t = 100)(\mu m)$	7.97001	7.9691	7.9689	7.9688	7.95
E(mms)	1.17	0.51	0.30	0.2	–

solidification at first (Alexiades, 1992) but it became a well-known bench mark for boiling simulation (Guo et al., 2011; Hardt and Wondra, 2008; Welch and Wilson, 2000). However, it can be conducted as a validation case for any one dimensional phase change phenomenon. In present study, Stefan problem is solved to validate condensation. The schematic of Stefan problem for condensation process is illustrated in Fig. 1. Heat is transferred by conduction from saturated vapor phase to liquid phase and it is rejected through subcooled wall. The vapor phase condensation leads to a motion of the interface to the right. It is assumed that during the condensation process the interface stays flat. Hence, the problem can be regarded as one-dimensional. The analytical solution of this problem is given by (Welch and Wilson, 2000):

$$x(t) = 2\eta\sqrt{d_L t} \tag{19}$$

where x is the interface position from cold wall, d_L is the liquid thermal diffusivity and η is determined from:

$$\eta \exp\left(\eta^2\right) erf(\eta) = \frac{c_{pL}(T_{sat} - T_{wall})}{\sqrt{\pi} H_{LG}} \tag{20}$$

where H_{LG} and c_{pL} is latent heat and liquid specific heat, respectively and *erf* is the error function.

A quasi 1D computational domain with only one grid cell in the direction of translational invariance is considered. The

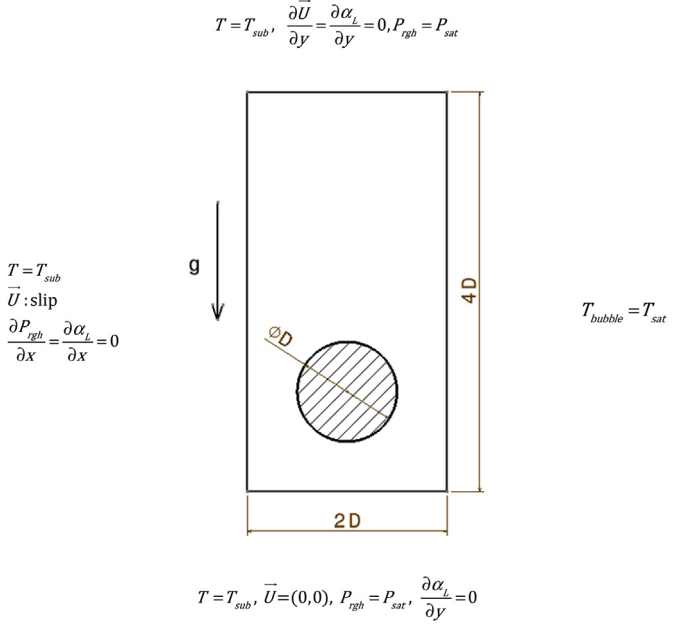

Fig. 3. Schematic of bubble condensation in subcooled boiling, initial and boundary conditions.

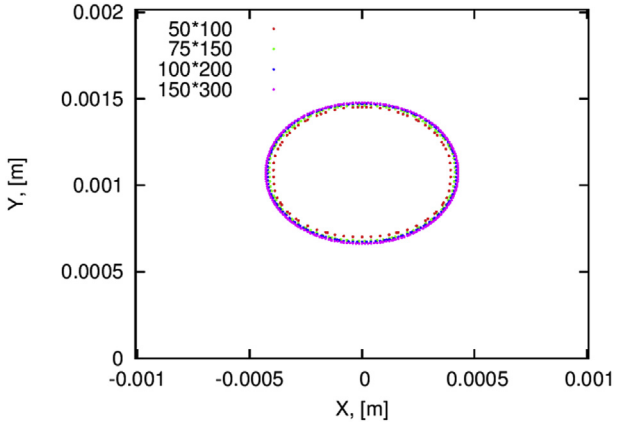

Fig. 4. Bubble shape at t = 1 *ms* for different grids, P_{sat} = 0.130[Mpa] and ΔT_{sub} = 25[K].

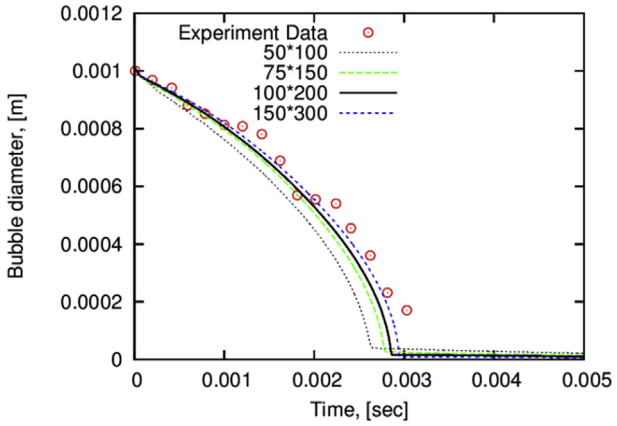

Fig. 5. Bubble diameter history, compare between present numerical simulations on different grids and experimental data (Kamei and Hirata, 1990a,b), D_0 = 1.008 mm, P_{sat} = 0.130[Mpa] and ΔT_{sub} = 25[K].

27

Longkai GUO

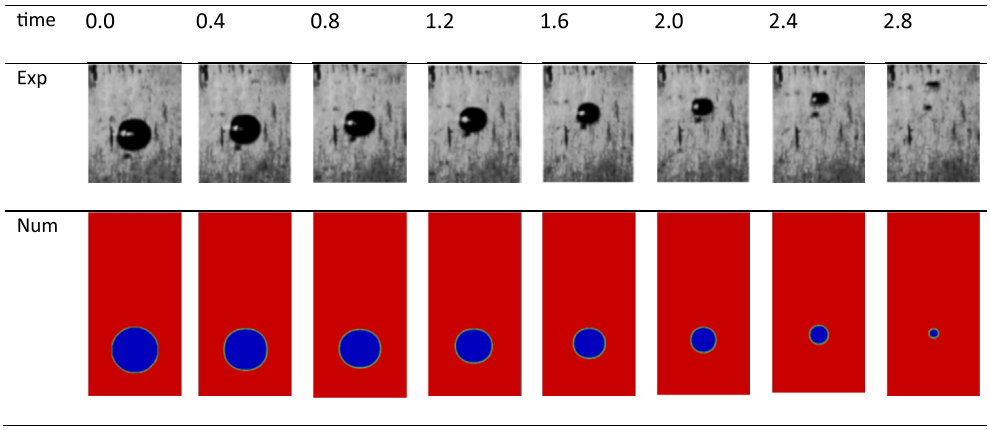

Fig. 6. Bubble shape, comparison between present numerical result and experimental data (Kamei and Hirata, 1990a,b), $D_0 = 1.008$ mm, $P_{sat} = 0.130$[MPa] and $\Delta T_{sub} = 25$[K].

liquid–vapor thermo physical properties for water at saturation pressure 0.130 MPa is chosen and displayed at Table 2. In order to ensure that the coefficient of mass flux in energy equation is consistent in CFD model during phase change process, liquid and vapor phases specific heat are assumed equal ($C_{pG} = C_{pL}(P_{sat})$). No slip boundary condition is employed for velocity boundary condition at the walls. Temperature of cold wall is 10° less than saturation temperature.

28 Longkai GUO

Since there is no sharp interface at color function VOF, iso-contour $\alpha_L = 0.5$ is applied as interface. Result of the comparison between exact solution and CFD model for Stefan problem is depicted in Fig. 2.

29 Longkai GUO

The integrated simulation error can be estimated as the film thickness error ($|\delta_{sim} - \delta_{an}|$) summed over time steps$i$, weighted by $\Delta t = 1E{-}05$(see Table 2).

$$E = \sum_i |\delta_{sim} - \delta_{an}| \Delta t \tag{21}$$

30-31 2 notes: There is an excellent agreement between present numerical result and exact solution based on illustrated result in Fig. 2 and Table 3.

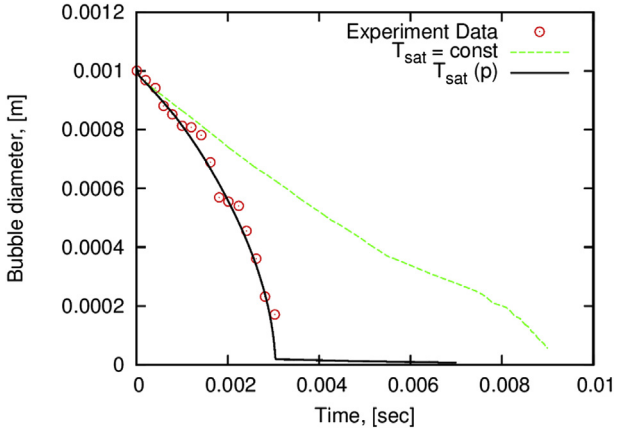

Fig. 7. Comparison of bubble diameter history, fixed saturation temperature vs variable saturation temperature based on local pressure, experiment data is provided by (Kamei and Hirata, 1990a,b).

3. Result and discussion

3.1. Problem description and validation

In present study, the rising of a single vapor bubble in quiescent subcooled water is simulated. The geometry of the considered problem is illustrated in Fig. 3. The 2-dimensional space domain is set as $2D_0 \times 4D_0$ where D_0 is the initial diameter of vapor bubble. The bubble is located in the position of (D_0,D_0) at the beginning of simulation. It should be noted that the solver is capable of 3D simulation. In order to simulate 2D simulation using OpenFOAM, special boundary condition called empty is applied in front and back faces.

3.2. Mesh resolution dependence

A mesh resolution analysis is performed on 4 different grids to figure out the appropriate grid size for simulation of bubble condensation in Fig. 4. These grids are 50 × 100, 75 × 150, 100 × 200 and 150 × 300 which respectively represent 25, 37, 50 and 75 cells across the initial diameter. It is obviously seen that bubble shape becomes converged with mesh 100 × 200 and 150 × 300. The variation among two lateral grids is negligible. Therefore the bubble is resolved using 100 × 200 cells in this study.

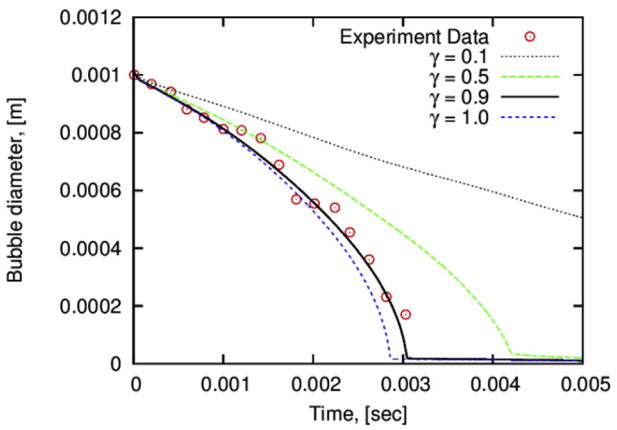

Fig. 8. The influence of mass transfer coefficient (γ) in Tanasawa model on CFD result. Experimental data of bubble condensation at $D_0 = 1.008$ mm, $P_{sat} = 0.130$[MPa] and $\Delta T_{sub} = 25$[K] is from (Kamei and Hirata, 1990a,b).

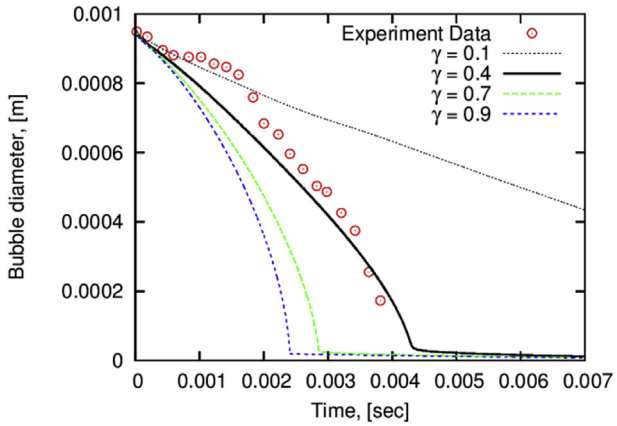

Fig. 9. The influence of mass transfer coefficient (γ) in Tanasawa model on CFD result. .Experimental data of bubble condensation at $D_0 = 0.95$ mm, $P_{sat} = 0.101$[MPa] and $\Delta T_{sub} = 12.8$[K] is from (Kamei and Hirata, 1990a,b).

3.3. Validation of bubble condensation

In order to validate present numerical simulation, the shape and the bubble diameter history is compared with published experimental results (Kamei and Hirata, 1990a,b) under saturation pressure 0.130 MPa. Thermo physical properties are displayed in Table 2. The comparison of bubble diameter history is shown in Fig. 5 and the bubble shape at Fig. 6. Bubble diameter in 2D simulation is the diameter of equivalent circle. It can be seen that numerical result is in reasonable good agreement with the experimental results.

3.4. Discussion on the single bubble condensation simulation

Even the rising of a single vapor bubble in quiescent subcooled water is a complex phenomenon. The mass transfer flux is proportional with the difference of vapor local saturation temperature with bulk liquid temperature. Local saturation temperature is a function of thermodynamic pressure which is non-uniform in quiescent water due to surface tension and gravity. Surface tension causes higher pressure in vapor bubble than surrounding liquid and gravity increases liquid pressure proportional to water column depth. Furthermore, various forces act on bubble such as capillary and buoyancy resulting different regimes of bubble.

From numerical point, real time simulation of two phase flow with phase change is a challenging task. For instance, the difference in the values of thermo physical properties across the narrow interface is high; the ratio of density $\frac{\rho_L}{\rho_G}$ in present simulation is about 1263. Moreover, for precise computation of mass flux in phase change process, an accurate mass transfer model is required. Some mass transfer models such as Tanasawa (Tanasawa, 1991) and Lee (Lee, 1980) are semi-experimental correlation and must be tuned up for numerical simulation using experimental data. Furthermore, accurate interface tracking method is necessary to compute surface tension force on vapor bubble interface correctly. The poor estimation of interface curvature causes unphysical spurious current near interface which may impair the mass flux calculation. Unfortunately, recent published articles (Bahreini et al., 2015) (Pan et al., 2012; Zeng et al., 2015) in this field have not addressed these issues. In this section the importance of different aspects of numerical parameters on final CFD result is discussed.

3.4.1. Local saturation temperature

To study the influence of local saturation temperature on the numerical result, the test case similar to previous section is carried out using constant saturation temperature for vapor; the result is compared with experimental data in Fig. 7. It shows when $T_{sat} = const$ is assumed, bubble diameter reduces almost linearly; because the temperature difference between saturated vapor bubble and subcooled water is constant during simulation. The area

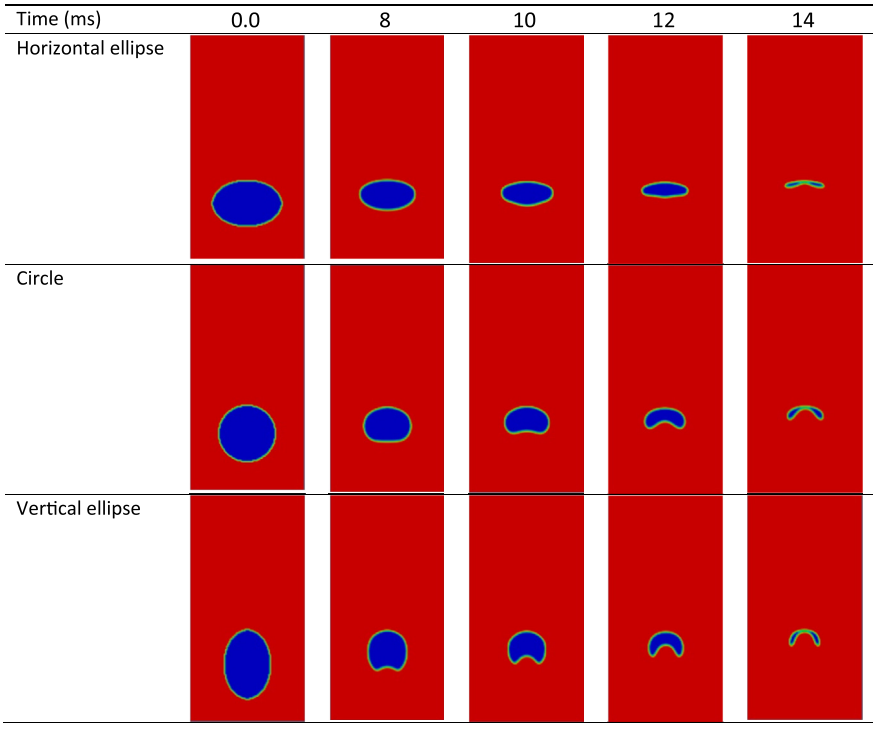

Fig. 10. Bubble shape sequences in condensation process started from different initial shape, $\Delta T = 25k$, $P_{sat} = 0.130$ MPa, $D_0 = 8$ mm.

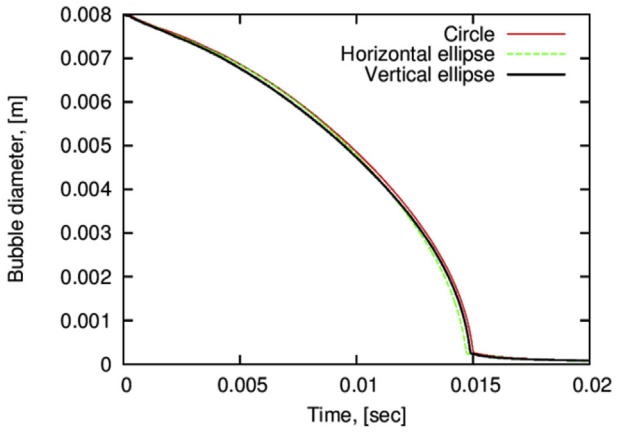

Fig. 11. Bubble diameter history, $\Delta T = 25k$, $P_{sat} = 0.130$ MPa, $D_0 = 8$ mm.

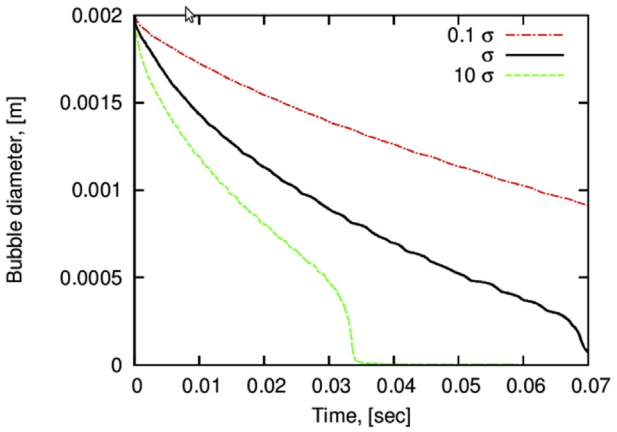

Fig. 13. The effect of spurious current magnitude on bubble life history, $\sigma = 0.05753$ N/m.

to volume ratio is becoming bigger in small bubble diameter; therefore, bubble is condensing faster in last stage. However, while a bubble is getting smaller in condensation process, the bubble inside pressure is increasing. Hence, if saturation temperature is computed as a function of thermodynamic pressure, it is slightly increased and accelerates bubble condensation. In the present study, the small variation of local saturation temperature due to pressure is calculated using Clausius–Clapeyron relation (equation (12)).

35-36
2 notes:

3.4.2. Mass transfer coefficient

The importance of variable γ in Tanasawa phase change model is investigated by comparison of bubble diameter history corresponding different value of γ in Fig. 8. $\gamma = 0.9$ is suitable for present simulation. When a vapor molecule collides on interface, it may reflect from interface or convert to liquid molecule. $\gamma = 0.9$ means 90% of vapor molecules are converting to the liquid and the remain is reflecting. The result shows bubble diameter history derived from numerical data is highly sensitive to mass transfer coefficient. Another drawback of Tanasawa phase change model is that mass transfer coefficient is a function of temperature and pressure. As seen in Fig. 9, for the vapor bubble condensation at saturation pressure 0.101 MPa and subcooled temperature 12.8 K, suitable value of γ is around 0.4. The reason is that smaller fraction of vapor molecules convert to liquid molecules while

37
Longkai GUO

38-39
2 notes:

40
Longkai GUO

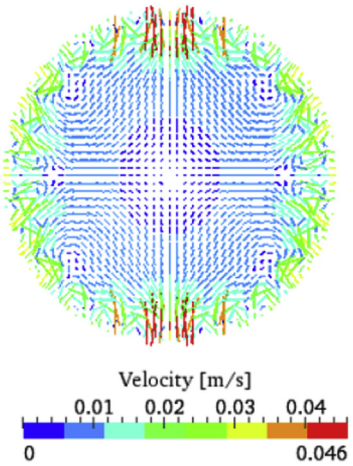

41
Longkai GUO

Fig. 12. Spurious currents in the vicinity of interface vapor bubble in zero gravity condition, $\Delta T = 25k$, $P_{sat} = 0.130$ MPa, $T_{sat} = const.$

hitting the interface at the lower saturation pressure and subcooled temperature. Hence, the value of mass transfer coefficient should be re-evaluated in each simulation by comparing it with experimental data. However, in this study the value of $\gamma = 0.9$ is employed for the rest of simulations, it is assumed the dependence of γ to subcooled temperature is negligible.

3.4.3. Effect of initial shape

It is assumed in CFD model that bubble initial shape is circle. It is often true for small bubbles, where surface tension is predominant and deviation of bubble shape from circularity is small. But the deviation can be big in large bubbles and it may affect the numerical result and lead to the wrong interpretation while comparing with experimental data. In this section, 3 different initial shapes of bubble (circle, horizontal ellipse and vertical ellipse) are compared with each other in Fig. 10 and Fig. 11. These bubbles have the same area. The elliptic shape is defined as:

$$\frac{(x-x_0)^2}{m^2} + \frac{(y-y_0)^2}{n^2} = \frac{D_0^2}{4nm} \tag{22}$$

where for horizontal ellipse ($m = 1$, $n = 1.5$) and for vertical ($m = 1.5$, $n = 1$) is considered.

The CFD result shows bubble shape sequences obviously vary due to different initial shape, but the bubble life time history is not sensitive to initial shape.

3.4.4. Spurious current

The interfacial tension force has been applied to Eulerian grids using different approaches a) continuous surface stress (CSS) method (Gueyffier et al., 1999), b) continuous surface force (CSF) (Brackbill et al., 1992) method and finally (c) sharp surface force (SSF) (Renardy and Renardy, 2002). In present study, CFS model is employed. However, an often reported problem of all these implementations (Brackbill et al., 1992; Gueyffier et al., 1999; Renardy and Renardy, 2002) is the existence of spurious currents in the flow field of the numerical simulations in the vicinity of the interface. In order to investigate the influences of spurious current on CFD results, the condensation of a single vapor bubble in zero gravity in quiescent subcooled water is simulated. In the absence of external force, flow must be still and motionless. Heat transfers from saturation vapor bubble to subcooled water by conduction heat mode and moves the interface. Spurious currents generate small vortex near interface as seen in Fig. 12. These small currents increase the heat transfer coefficient and lead to extra mass flux

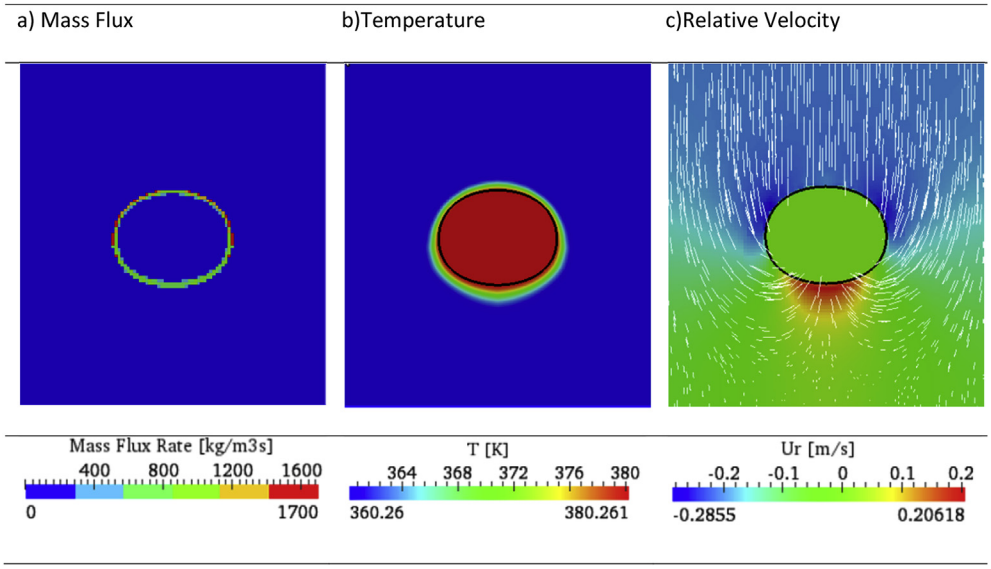

Fig. 14. Contour of mass flux, temperature and relative velocity of bubble condensation at $P_{sat} = 0.130$ MPa, $\Delta T = 20$ K, $D = 4$ mm.

across the interface. In this series of simulation, saturation temperature is assumed constant to omit the effect of pressure inside bubble on life time history. As seen in the Fig. 13, bubble life time reduces by the increase in the surface tension value. Because the magnitude of largest spurious currents around a bubble is linear proportional with the magnitude of surface tension (Lafaurie et al., 1994). This test shows the significant influences of unphysical spurious current on the numerical simulations of the single vapor bubble condensation.

Here, a smoothing filter method (equation (8)) is applied which improves interface curvature calculation and reduces the spurious current magnitude in one order. The filter makes remedy the problem but it cannot totally fade it out.

42

Longkai GUO

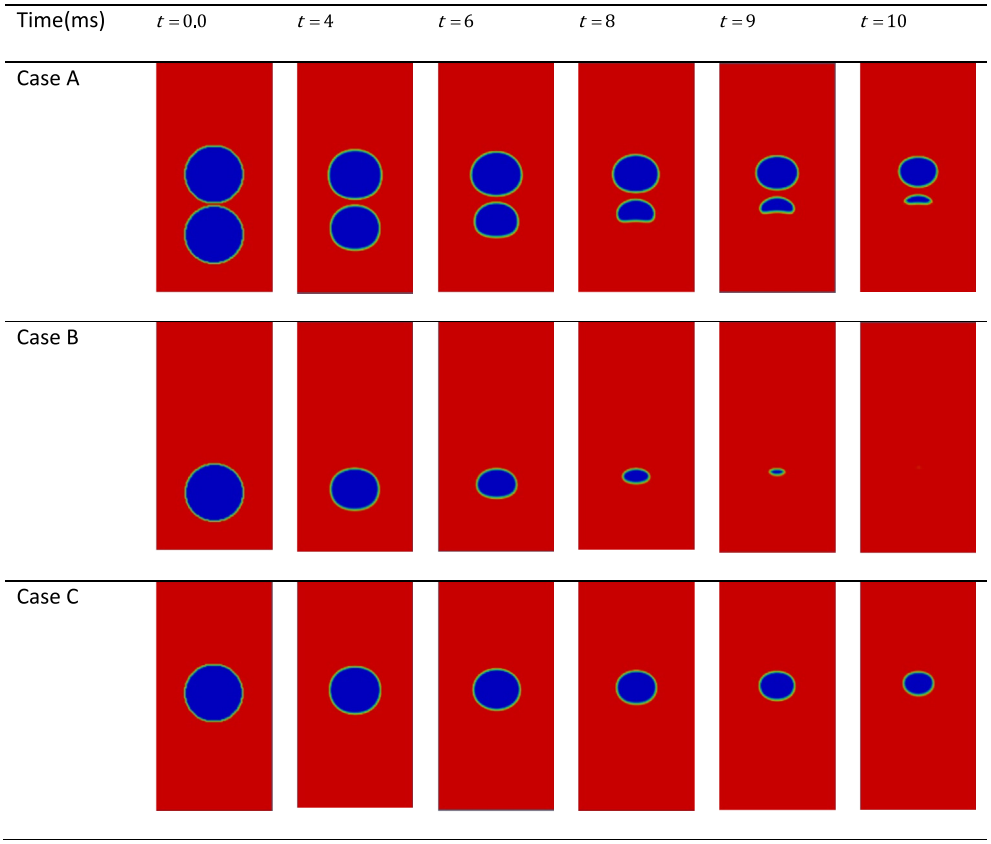

Fig. 15. Vapor bubble condensation at $P_{sat} = 0.130$ MPa, $\Delta T = 20$ K, $D = 4$ mm.

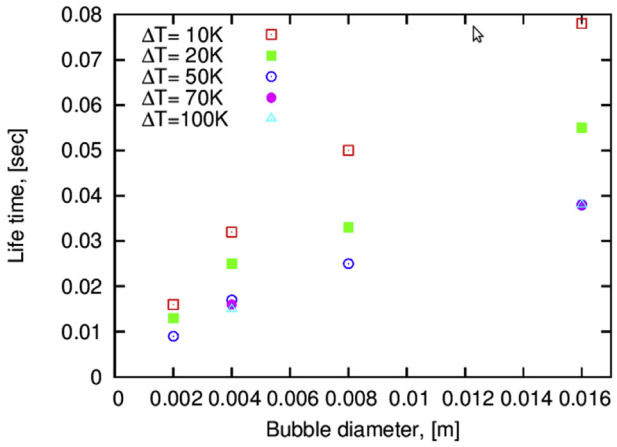

43

Longkai GUO **Fig. 16.** Bubble life time for different sizes of bubble at P_{Sat} = 0.130 MPa, ΔT is subcooled temperature.

3.5. Bubble condensation

3.5.1. Single bubble condensation

In the condensation process of vapor bubble, mass flux is higher in frontal face of bubble as illustrated in Fig. 14, because it is in exposure of lower subcooled temperature and higher relative velocity. Relative velocity is defined as:

44

Longkai GUO

$$\overrightarrow{U_r} = \overrightarrow{U} - \overrightarrow{U_b} \tag{23}$$

where $\overrightarrow{U_b}$ is bubble velocity computed from bubble mass center displacement. The relative velocity is downward in the front of bubble. In lateral sides of bubble front face, relative velocity reaches maximum value. It increases heat convection coefficient and produces higher mass flux. In the back face of bubble, relative velocity is upward. It is higher in the middle part of back face. A thin thermal boundary layer is generated in the behind of condensing vapor bubble, thus, subcooled temperature reduces leading to lower mass flux at back face.

3.5.2. Multiple bubble condensation

The Fig. 15 shows the performance of multiple vapor bubbles condensation on each single bubble. Three simulations are conducted in this section. In case A, two similar vapor bubbles are placed in computational domain at the beginning of simulation. The distance between bubbles centre is $1.1D_0$. In cases B and C the condensation of each lateral bubble are considered separately. Since thermodynamic pressure increases by water column depth, local saturation temperature is higher in deeper side. Hence, lower bubble experiences higher mass flux and condensates faster (compare Fig. 15-Case B and 15-Case C). The comparison of Fig. 15-Case A and 15-Case B indicates when a bubble moves afterward another bubble; the lower bubble life time becomes longer. Despite of single vapor bubble condensation, in this situation, the lower bubble is placed in the thermal boundary layer of above bubble. Thus, it is in exposure of less subcooled water which leading to smaller mass flux and longer life time.

3.5.3. Bubble life time

In a single vapor bubble condensation, bubble life time is dependent to bubble size and subcooled temperature. Fig. 16 indicates bubble size increases life time almost linearly. Fig. 17 shows the bubble shape sequences corresponding to different subcooled temperature value. It is found clearly that increase in the subcooled temperature decreases bubble life time. However, there is no linear relationship between bubble life time and subcooled temperature. Present numerical simulations in Fig. 18 indicates that the bubble life time has a rapidly decrease in the low subcooled degree region,

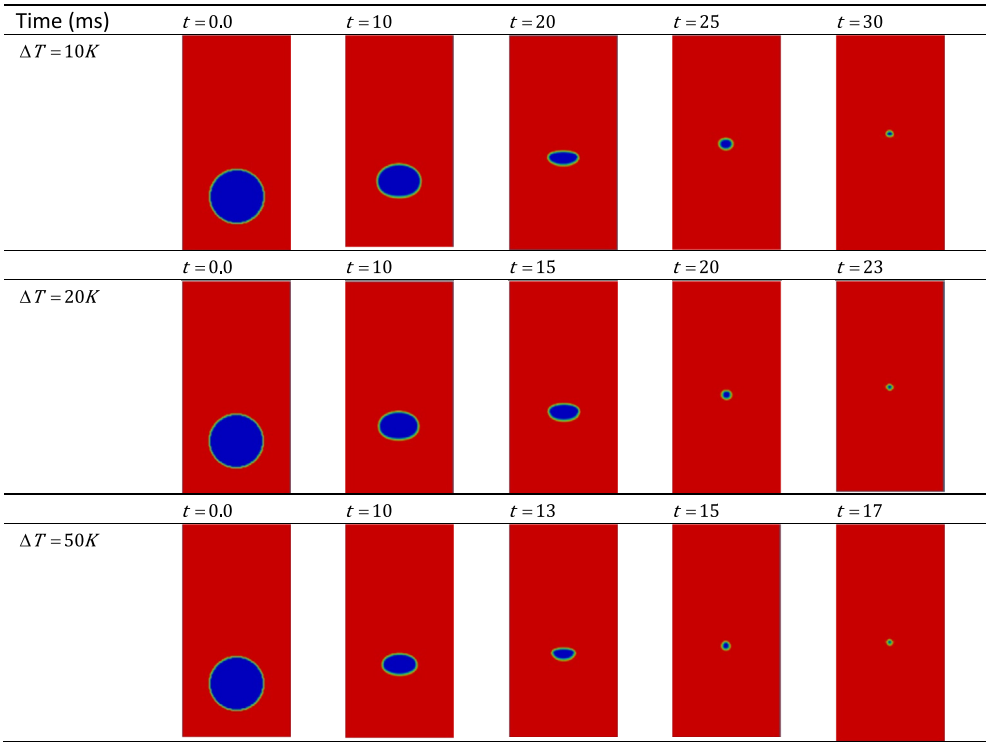

Fig. 17. Bubble shape sequences for condensation process atP_{sat} = 0.130 MPa, D_0 = 4 mm, ΔT is subcooled temperature.

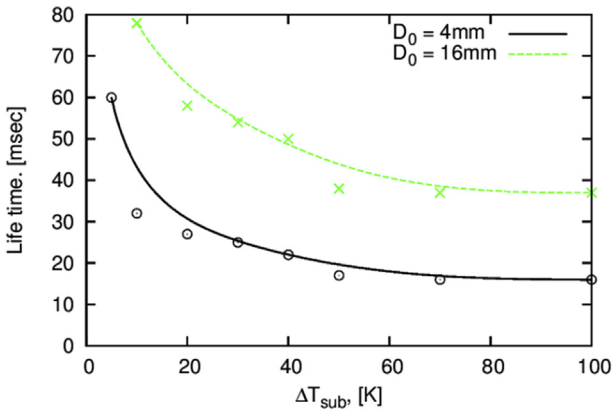

Fig. 18. Bubble life time vs. subcooled temperature at $P_{sat} = 0.130$ MPa.

but tends to be steady as the subcooled degree is large enough. Zeng et al. (Zeng et al., 2015) have been noted that once subcooled degree changes, the fluid thermodynamic properties changes as well, which thus leads to a non-linear relation between bubble life time and the subcooled degree. However, it seems this behavior returns to temporal scale of problem. The total heat capacity can be transferred using conduction and convection mode in a definite portion of time is limited. Hence, in low subcooled temperature, increase in subcooled temperature increases transferred heat across the interface but in large subcooled temperature, it has no effect either on transferred heat or mass flux. Thus, bubble life time in large subcooled region become steady. This numerical result is consistent with Sudhoff correlations (Sudhoff et al., 1982) which is a semi-empirical correlation on the basis of literature reviews.

45 Longkai GUO

4. Concluding remarks

In present study, condensation of vapor bubble in subcooled water is modeled using CF-VOF method in OpenFOAM solver (interFoam). In order to simulate phase change process, energy equation, Tanasawa mass transfer model and appropriate source terms are added to base solver. Implemented code is validated with analytical solution of Stefan problem, and then applied for simulation of a single and multiple vapor bubbles condensation. A single vapor bubble shape and life time history in condensation is verified with the experimental data (Kamei and Hirata, 1990a,b). The limitations of mass transfer model and numerical method are discussed exclusively. Furthermore, some promising remarks are obtained:

46

Longkai GUO 1 The main limitation of bubble condensation simulation using interface tracking method such as VOF is spurious current. It impairs numerical result by false extra heat convection near interface leading to increase in mass flux.

47 Longkai GUO

2 Despite the extensive use of Tanasawa mass transfer model for simulation of phase change (Hardt and Wondra, 2008; Magnini et al., 2013; Ranjan et al., 2011), this model is not recommended for simulation of bubble condensation in the absence of experimental data. Our study shows CFD results are highly sensitive to mass transfer coefficient γ and must be tuned up with experimental data for different working conditions.

3 The bubble life time is linearly dependent to bubble size and not sensitive of initial bubble shape. It has a non linear dependence to subcooled temperature. The influence of subcooled temperature variation in bubble life time is higher in low subcooled temperature. In enough large subcooled temperature, bubble life time is almost insensitive to subcooled temperature changes.

4 In a single vapor bubble condensation in quiescent water, mass flux is higher in the front face of bubble than back face.

5 Thermal boundary layer in bubble swarm motion prolongs lower bubbles condensation.

References

Alexiades, V., 1992. Mathematical Modeling of Melting and Freezing Processes. CRC Press.
Bahreini, M., Ramiar, A., Ranjbar, A.A., 2015. Numerical simulation of bubble behavior in subcooled flow boiling under velocity and temperature gradient. Nucl. Eng. Des. 293, 238–248.
Berberović, E., Hinsberg, N.P.V., Jakirlić, S., Roisman, I.V., Tropea, C., 2009. Drop impact onto a liquid layer of finite thickness: dynamics of the cavity evolution. Am. Phys. Soc. 79, 036306–036315.
Brackbill, J.U., Kothe, D.B., Zemach, C., 1992. A continuum method for modeling surface tension. J. Comput. Phys. 100, 335–354.
Brucker, G., Sparrow, E., 1977. Direct contact condensation of steam bubbles in water at high pressure. Int. J. Heat Mass Transf. 20, 371–381.
Chen, R., Tian, W., Su, G., Qiu, S., Ishiwatari, Y., Oka, Y., 2010. Numerical investigation on bubble dynamics during flow boiling using moving particle semi-implicit method. Nucl. Eng. Des. 240, 3830–3840.
Chen, R., Tian, W., Su, G., Qiu, S., Ishiwatari, Y., Oka, Y., 2011. Numerical investigation on coalescence of bubble pairs rising in a stagnant liquid. Chem. Eng. Sci. 66, 5055–5063.
Chen, Y., Mayinger, F., 1992. Measurement of heat transfer at the phase interface of condensing bubbles. Int. J. Multiph. Flow 18, 877–890.
Deshpande, S.S., Anumolu, L., Trujillo, M.F., 2012. Evaluating the performance of the two-phase flow solver interFoam. Comput. Sci. Discov. 5, 014016.
Gueyffier, D., Li, J., Nadim, A., Scardovelli, R., Zaleski, S., 1999. Volume-of-fluid interface tracking with smoothed surface stress methods for three-dimensional flows. J. Comput. Phys. 152, 423–456.
Guo, D.Z., Sun, D.L., Li, Z.Y., Tao, W.Q., 2011. Phase change heat transfer simulation for boiling bubbles arising from a vapor film by the VOSET method. Numer. Heat. Transf. 59, 857–881.
Harada, T., Nagakura, H., Okawa, T., 2010. Dependence of bubble behavior in sub-cooled boiling on surface wettability. Nucl. Eng. Des. 240, 3949–3955.
Hardt, S., Wondra, F., 2008. Evaporation model for interfacial flows based on a continuum-field representation of the source terms. J. Comput. Phys. 227, 5871–5895.
Hoang, D.A., van Steijn, V., Portela, L.M., Kreutzer, M.T., Kleijn, C.R., 2013. Benchmark numerical simulations of segmented two-phase flows in microchannels using the volume of fluid method. Comput. Fluids 86, 28–36.
Issa, R.I., Gosman, A., Watkins, A., 1986. The computation of compressible and incompressible recirculating flows by a non-iterative implicit scheme. J. Comput. Phys. 62, 66–82.
Jasak, H., 1996. Error Analysis and Estimation for the Finite Volume Method with Applications to Fluid Flows. University of London.
Kamei, S., Hirata, M., 1990a. Condensing phenomena of a single vapor bubble into subcooled water. Exp. Heat Transf. Int. J. 3, 173–182.
Kamei, S., Hirata, M., 1990b. Study on condensation of a single vapor bubble into subcooled water-Part 2; experimental analysis. Heat Trans. Jpn. Res. (USA) 19.
Klostermann, J., Schaake, K., Schwarze, R., 2013. Numerical simulation of a single rising bubble by VOF with surface compression. Int. J. Numer. Methods Fluids 71, 960–982.
Lafaurie, B., Nardone, C., Scardovelli, R., Zaleski, S., Zanetti, G., 1994. Modelling merging and fragmentation in multiphase flows with SURFER. J. Comput. Phys. 113, 134–147.
Lee, H., Kharangate, C.R., Mascarenhas, N., Park, I., Mudawar, I., 2015. Experimental and computational investigation of vertical downflow condensation. Int. J. Heat Mass Transf. 85, 865–879.
Lee, W.H., 1980. A pressure iteration scheme for two-phase flow modeling. Multiph. Transp. Fundam. React. Saf. Appl. 1, 407–431.
Lucas, D., Prasser, H.-M., 2007. Steam bubble condensation in sub-cooled water in case of co-current vertical pipe flow. Nucl. Eng. Des. 237, 497–508.
Magnini, M., Pulvirenti, B., Thome, J.R., 2013. Numerical investigation of hydrodynamics and heat transfer of elongated bubbles during flow boiling in a microchannel. Int. J. Heat Mass Transf. 59, 451–471.
Marek, R., Straub, J., 2001. Analysis of the evaporation coefficient and the condensation coefficient of water. Int. J. Heat Mass Transf. 44, 39–53.
Pan, L.-m., Tan, Z.-w., Chen, D.-q., Xue, L.-C., 2012. Numerical investigation of vapor bubble condensation characteristics of subcooled flow boiling in vertical rectangular channel. Nucl. Eng. Des. 248, 126–136.
Ranjan, R., Murthy, J.Y., Garimella, S.V., 2011. A microscale model for thin-film evaporation in capillary wick structures. Int. J. Heat Mass Transf. 54, 169–179.
Renardy, Y., Renardy, M., 2002. PROST: a parabolic reconstruction of surface tension for the volume-of-fluid method. J. Comput. Phys. 183, 400–421.
Rhie, C., Chow, W., 1983. Numerical study of the turbulent flow past an airfoil with trailing edge separation. AIAA J. 21, 1525–1532.
Rusche, H., 2003. Computational Fluid Dynamics of Dispersed Two-phase Flows at

High Phase Fractions. Imperial College London (University of London).
Samkhaniani, N., Ajami, A., Kayhani, M.H., Dari, A.S., 2012. Direct numerical simulation of single bubble rising in viscous stagnant liquid. In: International Conference on Merchanical, Automobile and Robotics Engineering (ICMAR'2012).
Samkhaniani, N., Gharehbaghi, A., Ahmadi, Z., 2013. Numerical simulation of reaction injection molding with polyurethane foam. J. Cell. Plastics 49, 405–421.
Scardovelli, R., Zaleski, S., 1999. Direct numerical simulation of free-surface and interfacial flow. Annu. Rev. Fluid Mech. 31, 567–603.
Sideman, S., Hirsch, G., 1965. Direct contact heat transfer with change of phase: condensation of single vapor bubbles in an immiscible liquid medium. Preliminary studies. AIChE J. 11, 1019–1025.
Sudhoff, B., Plischke, M., Weinspach, P., 1982. Direct contact heat transfer with change of phase-condensation or evaporation of a drobble. Ger. Chem. Eng. 5, 24–43.
Tanasawa, I., 1991. Advances in condensation heat transfer. Adv. Heat Transf. 21, 55–139.
Tian, W., Ishiwatari, Y., Ikejiri, S., Yamakawa, M., Oka, Y., 2010. Numerical computation of thermally controlled steam bubble condensation using Moving Particle Semi-implicit (MPS) method. Ann. Nucl. Energy 37, 5–15.
Van Leer, B., 1974. Towards the ultimate conservative difference scheme. II. Monotonicity and conservation combined in a second-order scheme. J. Comput. Phys. 14, 361–370.
Welch, S.W.J., Wilson, J., 2000. A volume of fluid based method for fluid flows with phase change. J. Comput. Phys. 160, 662–682.
Weller, H., 2008. A New Approach to VOF-based Interface Capturing Methods for Incompressible and Compressible Flow. OpenCFD Ltd. Report TR/HGW/04.
Weller, H.G., Taboral, G., Jasak, H., Fureby, C., 1998. A tensorial approach to computational continuum mechanics using object-oriented techniques. Comput. Phys. 12, 620–632.
Zalesak, S.T., 1979. Fully multidimensional flux-corrected transport algorithms for fluids. J. Comput. Phys. 31, 335–362.
Zeng, Q., Cai, J., Yin, H., Yang, X., Watanabe, T., 2015. Numerical simulation of single bubble condensation in subcooled flow using OpenFOAM. Prog. Nucl. Energy 83, 336–346.

Numerical simulation of bubble condensation using CF-VOF

Samkhaniani, N.; Ansari, M. R.

01 Longkai GUO Page 1
27/3/2019 15:05

02 Longkai GUO Page 1
27/3/2019 15:07

03 Longkai GUO Page 1
27/3/2019 15:07

04 Longkai GUO Page 1
27/3/2019 15:08

05 Longkai GUO Page 1
27/3/2019 15:09

06 Longkai GUO Page 1
27/3/2019 20:36

07 Longkai GUO Page 1
27/3/2019 20:35

08 Longkai GUO Page 1
27/3/2019 20:42

09 Longkai GUO Page 2
27/3/2019 20:50

10 Longkai GUO Page 2

27/3/2019 20:51

11 Longkai GUO Page 2

27/3/2019 20:53

12 Longkai GUO Page 2

27/3/2019 20:53

13 Longkai GUO Page 3

27/3/2019 20:54

14 Longkai GUO Page 3

27/3/2019 20:57

15 Longkai GUO Page 3

28/3/2019 8:57

16 Longkai GUO Page 3

28/3/2019 8:36

17 Longkai GUO Page 3

28/3/2019 8:37

18 Longkai GUO Page 3

28/3/2019 8:58

19 Longkai GUO Page 3

28/3/2019 8:58

20 Longkai GUO Page 3

28/3/2019 9:09

21 Longkai GUO Page 4

28/3/2019 9:17

22 Longkai GUO Page 4

28/3/2019 9:20

23 Longkai GUO Page 4

28/3/2019 9:18

24 Longkai GUO Page 4

28/3/2019 9:18

25 Longkai GUO Page 4

28/3/2019 9:34

26 Longkai GUO Page 4

28/3/2019 9:19

27 Longkai GUO Page 5

28/3/2019 9:40

28 Longkai GUO Page 6

28/3/2019 9:41

29 Longkai GUO Page 6

28/3/2019 10:13

30 Longkai GUO Page 6

28/3/2019 10:04

31 Longkai GUO Page 6

28/3/2019 10:14

32 Longkai GUO Page 7

28/3/2019 10:17

33 Longkai GUO Page 7

28/3/2019 10:19

34 Longkai GUO Page 7

28/3/2019 10:20

35 Longkai GUO Page 8

28/3/2019 10:23

36 Longkai GUO Page 8

28/3/2019 10:21

37 Longkai GUO Page 8

28/3/2019 10:22

38 Longkai GUO Page 8

28/3/2019 10:23

39 Longkai GUO Page 8

28/3/2019 10:24

40 Longkai GUO Page 8

28/3/2019 10:24

41 Longkai GUO Page 8

28/3/2019 10:25

42 Longkai GUO Page 9

28/3/2019 10:27

43 Longkai GUO Page 10

28/3/2019 10:30

44 Longkai GUO Page 10

28/3/2019 10:31

45 Longkai GUO Page 11

28/3/2019 10:32

46 Longkai GUO Page 11

28/3/2019 11:54

47 Longkai GUO Page 11

28/3/2019 11:55